The Astrophysical Journal, 954:88 (9pp), 2023 September 1 https://doi.org/10.3847/1538-4357/aced05

IXPE and XMM-Newton Observations of the Soft Gamma Repeater SGR 1806–20

Roberto Turolla[1,2], Roberto Taverna[1], Gian Luca Israel[3], Fabio Muleri[4], Silvia Zane[2], Matteo Bachetti[5], Jeremy Heyl[6], Alessandro Di Marco[4], Ephraim Gau[7], Henric Krawczynski[7], Mason Ng[8], Andrea Possenti[5], Juri Poutanen[9], Luca Baldini[10,11], Giorgio Matt[12], Michela Negro[13,14,15], Iván Agudo[16], Lucio A. Antonelli[17,18], Wayne H. Baumgartner[19], Ronaldo Bellazzini[10], Stefano Bianchi[12], Stephen D. Bongiorno[19], Raffaella Bonino[20,21], Alessandro Brez[10], Niccolò Bucciantini[22,23,24], Fiamma Capitanio[4], Simone Castellano[10], Elisabetta Cavazzuti[25], Chieng-Ting Chen[19,26], Stefano Ciprini[17,27], Enrico Costa[4], Alessandra De Rosa[4], Ettore Del Monte[4], Laura Di Gesu[25], Niccolò Di Lalla[28], Immacolata Donnarumma[25], Victor Doroshenko[29], Michal Dovčiak[30], Steven R. Ehlert[19], Teruaki Enoto[31], Yuri Evangelista[4], Sergio Fabiani[4], Riccardo Ferrazzoli[4], Javier A. Garcia[32], Shuichi Gunji[33], Kiyoshi Hayashida[34,55], Wataru Iwakiri[35], Svetlana G. Jorstad[36,37], Philip Kaaret[19,38], Vladimir Karas[30], Fabian Kislat[39], Takao Kitaguchi[31], Jeffery J. Kolodziejczak[19], Fabio La Monaca[4], Luca Latronico[21], Ioannis Liodakis[40], Simone Maldera[21], Alberto Manfreda[10], Frédéric Marin[41], Andrea Marinucci[25], Alan P. Marscher[36], Herman L. Marshall[8], Francesco Massaro[20,21], Ikuyuki Mitsuishi[42], Tsunefumi Mizuno[43], C.-Y. Ng[44], Stephen L. O'Dell[19], Nicola Omodei[28], Chiara Oppedisano[21], Alessandro Papitto[18], George G. Pavlov[45], Abel L. Peirson[28], Matteo Perri[17,18], Melissa Pesce-Rollins[10], Pierre-Olivier Petrucci[46], Maura Pilia[5], Simonetta Puccetti[17], Brian D. Ramsey[19], John Rankin[4], Ajay Ratheesh[4], Oliver J. Roberts[19,26], Roger W. Romani[28], Carmelo Sgró[10], Patrick Slane[47], Paolo Soffitta[4], Gloria Spandre[10], Douglas A. Swartz[19,26], Toru Tamagawa[31,48,49], Fabrizio Tavecchio[50], Yuzuru Tawara[42], Allyn F. Tennant[19], Nicholas E. Thomas[19], Francesco Tombesi[27,51,52], Alessio Trois[5], Sergey S. Tsygankov[9], Jacco Vink[53], Martin C. Weisskopf[19], Kinwah Wu[2], and Fei Xie[4,54]

[1] Dipartimento di Fisica e Astronomia, Università degli Studi di Padova, Via Marzolo 8, I-35131 Padova, Italy; turolla@pd.infn.it
[2] Mullard Space Science Laboratory, University College London, Holmbury St Mary, Dorking, Surrey RH5 6NT, UK
[3] INAF Osservatorio Astronomico di Roma, via Frascati 33, I-00078 Monteporzio Catone, Italy
[4] INAF Istituto di Astrofisica e Planetologia Spaziali, Via del Fosso del Cavaliere 100, I-00133 Roma, Italy
[5] INAF Osservatorio Astronomico di Cagliari, Via della Scienza 5, I-09047 Selargius (CA), Italy
[6] Department of Physics and Astronomy, University of British Columbia, Vancouver, BC V6T 1Z1, Canada
[7] Physics Department and McDonnell Center for the Space Sciences, Washington University in St. Louis, St. Louis, MO 63130, USA
[8] MIT Kavli Institute for Astrophysics and Space Research, Massachusetts Institute of Technology, 77 Massachusetts Avenue, Cambridge, MA 02139, USA
[9] Department of Physics and Astronomy, FI-20014 University of Turku, Finland
[10] Istituto Nazionale di Fisica Nucleare, Sezione di Pisa, Largo B. Pontecorvo 3, I-56127 Pisa, Italy
[11] Dipartimento di Fisica, Università di Pisa, Largo B. Pontecorvo 3, I-56127 Pisa, Italy
[12] Dipartimento di Matematica e Fisica, Università degli Studi Roma Tre, Via della Vasca Navale 84, I-00146 Roma, Italy
[13] University of Maryland, Baltimore County, Baltimore, MD 21250, USA
[14] NASA Goddard Space Flight Center, Greenbelt, MD 20771, USA
[15] Center for Research and Exploration in Space Science and Technology, NASA/GSFC, Greenbelt, MD 20771, USA
[16] Instituto de Astrofísica de Andalucía-CSIC, Glorieta de la Astronomía s/n, E-18008, Granada, Spain
[17] Space Science Data Center, Agenzia Spaziale Italiana, Via del Politecnico snc, I-00133 Roma, Italy
[18] INAF Osservatorio Astronomico di Roma, Via Frascati 33, I-00078 Monte Porzio Catone (RM), Italy
[19] NASA Marshall Space Flight Center, Huntsville, AL 35812, USA
[20] Dipartimento di Fisica, Università degli Studi di Torino, Via Pietro Giuria 1, I-10125 Torino, Italy
[21] Istituto Nazionale di Fisica Nucleare, Sezione di Torino, Via Pietro Giuria 1, I-10125 Torino, Italy
[22] INAF Osservatorio Astrofisico di Arcetri, Largo Enrico Fermi 5, I-50125 Firenze, Italy
[23] Dipartimento di Fisica e Astronomia, Università degli Studi di Firenze, Via Sansone 1, I-50019 Sesto Fiorentino (FI), Italy
[24] Istituto Nazionale di Fisica Nucleare, Sezione di Firenze, Via Sansone 1, I-50019 Sesto Fiorentino (FI), Italy
[25] Agenzia Spaziale Italiana, Via del Politecnico snc, I-00133 Roma, Italy
[26] Universities Space Research Association (USRA), USA
[27] Istituto Nazionale di Fisica Nucleare, Sezione di Roma Tor Vergata, Via della Ricerca Scientifica 1, I-00133 Roma, Italy
[28] Department of Physics and Kavli Institute for Particle Astrophysics and Cosmology, Stanford University, Stanford, CA 94305, USA
[29] Institut für Astronomie und Astrophysik, Universität Tübingen, Sand 1, D-72076 Tübingen, Germany
[30] Astronomical Institute of the Czech Academy of Sciences, Boční II 1401/1, 14100 Praha 4, Czech Republic
[31] RIKEN Cluster for Pioneering Research, 2-1 Hirosawa, Wako, Saitama 351-0198, Japan
[32] California Institute of Technology, Pasadena, CA 91125, USA
[33] Yamagata University, 1-4-12 Kojirakawa-machi, Yamagata-shi 990-8560, Japan
[34] Osaka University, 1-1 Yamadaoka, Suita, Osaka 565-0871, Japan
[35] International Center for Hadron Astrophysics, Chiba University, Chiba 263-8522, Japan
[36] Institute for Astrophysical Research, Boston University, 725 Commonwealth Avenue, Boston, MA 02215, USA
[37] Department of Astrophysics, St. Petersburg State University, Universitetsky pr. 28, Petrodvoretz, 198504 St. Petersburg, Russia
[38] University of Iowa, Department of Physics and Astronomy, Van Allen Hall, 30 North Dubuque Street, Iowa City, IA 52242, USA
[39] University of New Hampshire, Department of Physics & Astronomy, Space Science Center, Morse Hall, Room 311, 8 College Road, Durham, NH 03824, USA
[40] Finnish Centre for Astronomy with ESO, FI-20014 University of Turku, Finland
[41] Université de Strasbourg, CNRS, Observatoire Astronomique de Strasbourg, UMR 7550, F-67000 Strasbourg, France
[42] Graduate School of Science, Division of Particle and Astrophysical Science, Nagoya University, Furo-cho, Chikusa-ku, Nagoya, Aichi 464-8602, Japan
[43] Hiroshima Astrophysical Science Center, Hiroshima University, 1-3-1 Kagamiyama, Higashi-Hiroshima, Hiroshima 739-8526, Japan
[44] Department of Physics, The University of Hong Kong, Pokfulam, Hong Kong
[45] Department of Astronomy and Astrophysics, Pennsylvania State University, University Park, PA 16802, USA
[46] Université Grenoble Alpes, CNRS, IPAG, F-38000 Grenoble, France
[47] Center for Astrophysics, Harvard & Smithsonian, 60 Garden Street, Cambridge, MA 02138, USA

[48] RIKEN Nishina Center, 2-1 Hirosawa, Wako, Saitama 351-0198, Japan
[49] Department of Physics, Tokyo University of Science, 1-3 Kagurazaka, Shinjuku, Tokyo 162-8601, Japan
[50] INAF Osservatorio Astronomico di Brera, Via E. Bianchi 46, I-23807 Merate (LC), Italy
[51] Dipartimento di Fisica, Università degli Studi di Roma Tor Vergata, Via della Ricerca Scientifica 1, I-00133 Roma, Italy
[52] Department of Astronomy, University of Maryland, College Park, MD 20742, USA
[53] Anton Pannekoek Institute for Astronomy & GRAPPA, University of Amsterdam, Science Park 904, 1098 XH Amsterdam, The Netherlands
[54] Guangxi Key Laboratory for Relativistic Astrophysics, School of Physical Science and Technology, Guangxi University, Nanning 530004, People's Republic of China
Received 2023 June 15; revised 2023 July 30; accepted 2023 August 1; published 2023 August 25

Abstract

Recent observations with the Imaging X-ray Polarimetry Explorer (IXPE) of two anomalous X-ray pulsars provided evidence that X-ray emission from magnetar sources is strongly polarized. Here we report on the joint IXPE and XMM-Newton observations of the soft γ-repeater SGR 1806–20. The spectral and timing properties of SGR 1806–20 derived from XMM-Newton data are in broad agreement with previous measurements; however, we found the source at an all-time low persistent flux level. No significant polarization was measured apart from the 4–5 keV energy range, where a probable detection with PD $= 31.6\% \pm 10.5\%$ and PA $= -17.^{\circ}6^{+15.5}_{-15.0}$ was obtained. The resulting polarization signal, together with the upper limits we derive at lower and higher energies (2–4 and 5–8 keV, respectively), is compatible with a picture in which thermal radiation from the condensed star surface is reprocessed by resonant Compton scattering in the magnetosphere, similar to what was proposed for the bright magnetar 4U 0142+61.

Unified Astronomy Thesaurus concepts: Neutron stars (1108); Magnetars (992); Polarimetry (1278); X-ray sources (1822)

1. Introduction

Soft γ-repeaters (SGRs) and anomalous X-ray pulsars (AXPs) together form a small class of Galactic X-ray pulsars characterized by long spin periods ($P \sim 1$–12 s), high spin-down rates ($\dot{P} \sim 10^{-15}$–10^{-10} s s^{-1}), and emission of short, energetic bursts of hard X-/soft γ-rays. The huge inferred values of the (spin-down) dipole field ($B \sim 10^{13}$–10^{15} G), the lack of a detected binary companion, and a persistent X-ray luminosity, $L_X \sim 10^{30}$–10^{35} erg s^{-1}, typically in excess of the spin-down power indicate that these sources are magnetars, ultramagnetized neutron stars powered by their own magnetic energy (Duncan & Thompson 1992; Thompson & Duncan 1993; see also Turolla et al. 2015; Kaspi & Beloborodov 2017 for reviews and Olausen & Kaspi 2014 for a catalog of magnetar sources[56]).

Because of the superstrong magnetic fields they host, the opacities of the two normal polarization modes are very different, so the X-ray emission from SGRs/AXPs is expected to be highly polarized (up to ≈80%; Fernández & Davis 2011; Taverna et al. 2014, 2020; Caiazzo et al. 2022). Theoretical predictions were finally tested when the NASA-ASI Imaging X-ray Polarimetry Explorer (IXPE; Weisskopf et al. 2022), the first satellite designed to provide imaging polarimetry in the 2–8 keV band, observed the two brightest magnetar sources, the AXPs 4U 0142+61 and 1RXS J170849.0–400910 (hereafter 1RXS J1708), during the first year of operations. Polarization was clearly detected in the 2–8 keV band at the ≈13.5% level in the former and to a much higher degree, ≈35%, in the latter (Taverna et al. 2022; Zane et al. 2023).

In both sources, the polarization strongly depends on energy. In 1RXS J1708, it monotonically increases from ≈20% up to ≈80% at a constant polarization angle (PA), possibly indicating that 2–8 keV photons come from regions of the star surface with different properties: a magnetic condensate (either solid or liquid) and an atmosphere (Zane et al. 2023). On the other hand, in 4U 0142+61, it first decreases from ≈15% to zero at around 4–5 keV, where the PA swings by 90°, and then rises to ≈35%, suggesting that thermal radiation from a condensed surface patch is then reprocessed by resonant Compton scattering (RCS; Thompson et al. 2002; Fernández & Thompson 2007; Nobili et al. 2008) onto mildly relativistic electrons flowing in the star's twisted magnetosphere (Taverna et al. 2022; an alternative interpretation in terms of mode switching in a magnetized atmosphere was recently put forward by Lai 2023).

Polarization measurements in strongly magnetized neutron stars can probe vacuum birefringence, a strong-field, quantum electrodynamics (QED) effect predicted more than 80 yr ago but never experimentally tested as yet (see, e.g., Heyl & Shaviv 2000, 2002, and references therein). Although previous magnetar observations are in agreement with QED predictions, no smoking-gun evidence for vacuum birefringence was found, mostly because thermal emission in both 4U 0142+61 and 1RXS J1708 comes from a fairly limited area of the star surface, so its intrinsic polarization is preserved at infinity anyway, even if no vacuum birefringence is present (see van Adelsberg & Perna 2009; Santangelo et al. 2019).

Further magnetar observations with IXPE are required to address this issue and provide fresh insight into the similarities/differences among magnetar sources. Here we report on the simultaneous IXPE and XMM-Newton observations of the prototypical magnetar SGR 1806–20. The XMM-Newton and IXPE observations are detailed in Section 2, and the results of the timing, spectral, and polarimetric analyses are presented in Section 3. Discussion follows in Section 4.

2. Observations

First identified as a high-energy transient in the KONUS data over 40 yr ago (Mazets et al. 1981), SGR 1806–20 was shortly after realized to be a repeater (Atteia et al. 1987; Kouveliotou et al. 1987; Laros et al. 1987). The source, located about 8.7 kpc from the Sun (Bibby et al. 2008), is a regular and

[55] Deceased.
[56] Available online at http://www.physics.mcgill.ca/pulsar/magnetar/main.html.

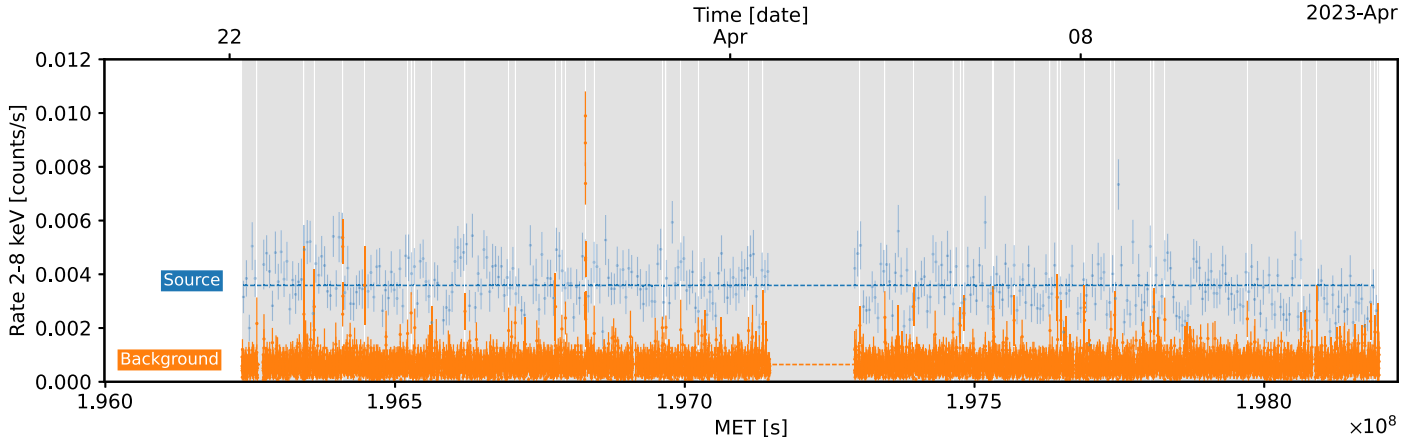

Figure 1. Count rate in the 2–8 keV energy range, summed over the three IXPE DUs, as a function of time for two regions in the field of view, one containing the source and the other only background. Periods in which the background was larger than 50% of the average source rate are identified by vertical white lines and removed by subsequent analyses. The time bin is 5000 and 100 s for the source and background, respectively.

prolific emitter of short bursts clustered in active periods, one of which occurred in 2004 and culminated on 2004 December 27 with the emission of the most powerful giant flare observed so far from a magnetar ($L \approx 10^{47}$ erg s^{-1}; Hurley et al. 2005; Palmer et al. 2005).

Object SGR 1806–20 spins with a period $P \approx 7.5$ s; the period derivative increased from $\dot{P} = 8 \times 10^{-11}$ s s^{-1} to 5×10^{-10} s s^{-1} in 2000–2011 and then went back to the "historical" value (see Younes et al. 2017). The latter implies a surface (dipole) field of $B = 8 \times 10^{14}$ G, the highest ever recorded. The steady X-ray emission in the 0.5–10 keV range, $L_X \approx 10^{35}$ erg s^{-1} (for the assumed distance of 8.7 kpc), is well described by the superposition of a blackbody (BB) and a power-law (PL) component with a (slightly variable) temperature $kT \approx 0.6$ keV, BB radius $\approx$ 1–2 km, and spectral index $\Gamma \approx 1.6$ (Mereghetti et al. 2005b; Woods et al. 2007; Younes et al. 2015, 2017). The PL tail extends, seemingly unbroken, into higher energies (up to $\approx$200 keV; see, e.g., Mereghetti et al. 2005a; Younes et al. 2017). The pulse profile is double-peaked with a pulsed fraction (PF) $\approx$ 3%–8% in a wide energy range (Woods et al. 2007; Younes et al. 2015, 2017).

The emission of a bright burst detected by several instruments on 2023 February 23 (Brivio et al. 2023; Mereghetti et al. 2023) marked the onset of a renewed period of activity from SGR 1806–20. To catch the source in an active state, IXPE observed SGR 1806–20 starting on 2023 March 22. In addition, a DDT pointing with XMM-Newton was activated.

2.1. XMM-Newton

Starting on 2023 April 7 00:18:48 UTC, SGR 1806–20 was observed with the European Photon Imaging Camera (EPIC) on board the XMM-Newton satellite for an exposure time of about 45 ks. The EPIC-pn (Strüder et al. 2001) was operating in full-frame mode (timing resolution of 73.4 ms). The MOS cameras (Turner et al. 2001) were set in small window mode (timing resolution of 0.3 s).

Standard procedures were applied in the extraction of the scientific products. Time intervals of high background activity were removed, resulting in a net exposure of 34.9 and 40.5 ks for the pn and MOSs, respectively. We collected the source photons from within a circle of radius 42″. The background level was estimated from a circular region of radius 100″ centered far from the source on the same CCD for the pn and, due to the reduced window, a different CCD for the MOSs. We checked for the potential impact of pileup with the EPATPLOT tool and found a negligible pileup fraction of $\approx$0.4%. The response matrices and ancillary files were generated by means of the RMFGEN and ARFGEN tasks, respectively. The final source spectra were obtained using SPECGROUP, rebinning the channels by a factor of 3 in order to match the intrinsic EPIC spectral resolution and imposing a minimum of 25 counts in each channel. Background-subtracted and exposure-corrected light curves were extracted using EPICLCCORR. The EPIC photon arrival times were referenced to the solar system barycenter. The source was found at a count rate of 0.354(3) counts s^{-1} (here and in the following, uncertainties are reported at a 1σ confidence level, unless specified otherwise).

2.2. IXPE

The IXPE observed SGR 1806–20 from 2023 March 22 05:57:51 UTC to 2023 April 1 18:56:26 UTC and from 2023 April 3 11:41:03 UTC to 2023 April 13 22:20:20 UTC for a total on-source time of $\approx$947 ks. Processed level 2 photon lists, one for each of the three IXPE detector units (DUs), were downloaded from the archive at HEASARC[57] and further processed to reduce the background with respect to the source signal.

Source and background counts were extracted from a circular region centered on the source position (identified with the brightest pixel in the IXPE image) with a radius of 36″ and a concentric annulus with inner and outer radii of 78″ and 240″, respectively. In order to discriminate the background events due to charged particles and high-energy photons without affecting the genuine X-ray events, we then applied the rejection criteria described in Di Marco et al. (2023). The counting rate as a function of time is shown in Figure 1. Time periods during which the background was larger than 50% of the source average counting rate are flagged and removed from the subsequent analysis. This step removes $\approx$6 out of the total $\approx$947 ks of the IXPE observation. Arrival times were corrected to the solar system barycenter with the FTOOL BARYCORR included in HEASOFT 6.31.1 using the Jet Propulsion

[57] https://heasarc.gsfc.nasa.gov/docs/ixpe/archive/

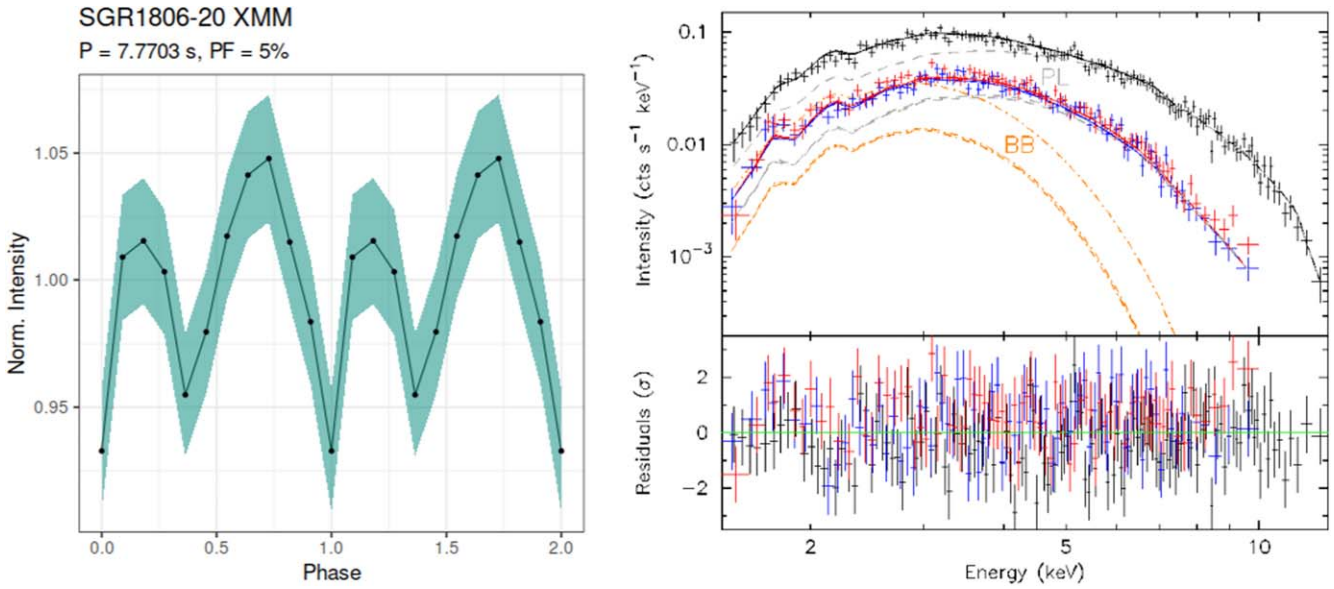

Figure 2. Left: joint XMM-Newton 1–12 keV EPIC-pn and MOS light curve folded to the best period inferred from the phase-fitting analysis (see text for details). The colored area marks the 1σ uncertainties on the data points. Right: EPIC-pn (black plus signs and lines), MOS1 (blue plus signs and lines), and MOS2 (red plus signs and lines) spectra of SGR 1806–20 (upper panel), together with the fitting residuals, in units of standard deviation (lower panel), for the BB+PL model discussed in the text. The individual BB and PL components are shown by an orange dashed–dotted and gray dashed line, respectively.

Laboratory Development Ephemeris 421 and the International Celestial Reference System frame.

3. Results

3.1. XMM-Newton Timing and Spectral Analysis

Both pn and MOS photon arrival time lists were used in order to look for the pulsar spin signal. We started from the timing properties inferred from the most recent spin measurements of SGR 1806–20 in 2015–2016 (Younes et al. 2017) and extrapolated them to the epoch of the new XMM-Newton data set. In particular, we assumed a spin period $P = 7.7501(2)$ s and a first period derivative $\dot{P} = 7.5(2) \times 10^{-11}$ s s^{-1}, both referred to MJD 57,202. The linear evolution of the period in 2015–2016 (see Figure 3 of Younes et al. 2017) and the relatively quiet behavior of the source in the last few years suggest that $\dot{P}$ has been constant (or at most slightly variable) since then. Correspondingly, we analyzed the new XMM-Newton data sets, searching for significant peaks in the 7.7659–7.7712 s period range, i.e., accounting for changes in P and $\dot{P}$ up to about 6σ with respect to the values reported by Younes et al. (2017).

Only one significant peak with a chance probability of about 9.6σ of not being a statistical fluctuation, and after having corrected for the number (530) of independent sampling periods of the search, was found in the Rayleigh periodogram. The period is 7.770 s. The modulation is present in both the pn and the MOS data alone, confirming that the signal is intrinsic to the source and not an instrumental artifact. In order to obtain a more refined measurement, we applied a phase-fitting technique, which resulted in a period of 7.7703(2) s (frequency $\nu = 0.128695(4)$ Hz); we also derived a 3σ upper limit on the period derivative, $|\dot{P}| < 2 \times 10^{-7}$ s s^{-1}. The 1–12 keV pulse shape is double-peaked, in agreement with the profiles obtained for SGR 1806–20 in the past (Younes et al. 2015). The PF (defined as the semiamplitude of the sinusoid divided by the source average count rate) is PF = 5(1)% (see left panel of Figure 2).

The spectral analysis of SGR 1806–20 was performed by simultaneously fitting all of the EPIC data sets within XSPEC (Arnaud 1996). A single-component (absorbed) model, such as a PL or BB, resulted in a poor fit (reduced $\chi^2 \approx 1.3$–3.1 for 300 dof). A BB+PL and a BB+BB model, often adopted to describe the 0.1–12 keV magnetar spectra, yield a good agreement with the data (reduced $\chi^2 \approx 1.17$ in both cases). The best-fitting parameters are listed in Table 1, and the EPIC spectra together with the best-fitting BB+PL model are shown in the right panel of Figure 2. We find that the addition of a second spectral component is significant to more than 6σ. Although the BB+BB and BB+PL models are equally acceptable on a statistical basis, in the following, we refer to the latter. The BB+PL spectral decomposition has been widely adopted in the past for SGR 1806–20, and this choice is motivated by the clear detection of a PL tail, e.g., in NuSTAR data (Younes et al. 2015, 2017). The inferred parameters are in agreement with the average values obtained in the past 10 yr, though the flux was unexpectedly a factor of about 3 lower than the average.

3.2. IXPE Timing and Spectropolarimetric Analysis

After background and solar flare removal (see Section 2.2), no significant changes in both the source and background counts were detected in the two IXPE pointings, so we used the combined data in our analysis.

We searched for pulsations using the Z_2^2 statistics (Buccheri et al. 1983), which is adequate for double-peaked pulsed profiles. We joined the event lists from the three DUs and ran the search using the quasi-fast folding algorithm described in Bachetti et al. (2020, 2021). We searched over spin frequencies between 0.125 and 0.129 Hz that contained the XMM-Newton solution and frequency derivatives $|\dot{\nu}_{\rm spin}| < 4 \times 10^{-12}$ Hz s^{-1}. Given the low number of source counts (see below), we did not find significant peaks in the search; we derived a 5.2% PF upper limit on pulsations over the frequency interval indicated above ($Z_2^2 \approx 25$; 90% confidence level, evaluated following

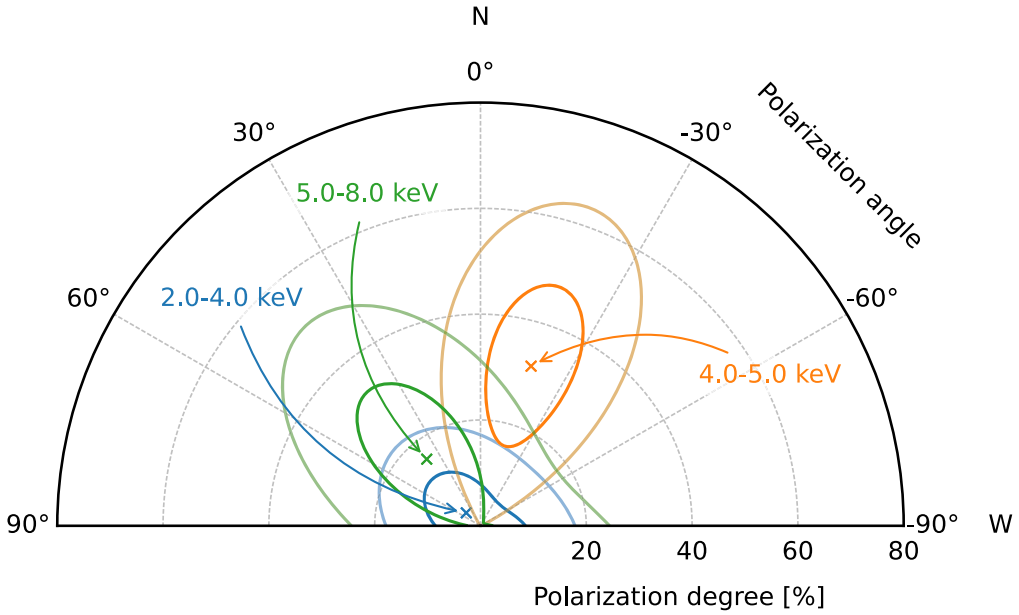

Figure 3. Contour plot of the IXPE PD and PA in different energy bands. The inner and outer contours mark the regions at the 68.3% and 99% confidence level, respectively. The spectral model is frozen to that obtained from the XMM-Newton observation.

Table 1
Results of the XMM-Newton Spectral Fits

Model	$N_{\rm H}$ (10^{22} cm^{-2})	$kT_{\rm BB_1}$ (keV)	$R_{\rm BB_1}$[a] (km)	Γ |$kT_{\rm BB_2}$ – | (keV)	Norm PL[b] |$R_{\rm BB_2}$[a] – | (km)	Flux[c] (Obs. | Unabs.) (10^{-12} erg cm^{-2} s^{-1})	χ^2/dof
BB+PL	6.5 ± 0.3	0.59 ± 0.04	$1.3^{+0.3}_{-0.2}$	1.7 ± 0.1	$(1.3 \pm 0.3) \times 10^{-3}$	4.3 ± 0.1 |11.3 ± 0.4	351.9/298
BB+BB	5.7 ± 0.2	0.70 ± 0.03	1.2 ± 0.1	2.4 ± 0.1	0.11 ± 0.01	4.3 ± 0.1 |8.2 ± 0.2	351.2/298

Notes. In the fifth and sixth columns, the bar is to separate the two entries (e.g. either Gamma or $kT_{\rm BB}$). The dash indicates that the corresponding quantity is dimensionless.
[a] Derived by adopting an 8.7 kpc distance (Bibby et al. 2008).
[b] In units of counts keV^{-1} cm^{-2} s^{-1}.
[c] The fluxes are estimated in the 0.5–10 keV energy range.

Vaughan et al. 1994). This upper limit is compatible with the detection with XMM-Newton of an ≈5% PF.

We extracted the Stokes parameters I, Q, and U with the `xpbin` tool, exploiting the weighted analysis method (Di Marco et al. 2022) implemented in the latest version (30.3) of the IXPEOBSSIM software (Baldini et al. 2022).[58] As a consequence of the limited number of counts (≈8000 background-subtracted events in the three DUs), the phase- and energy-integrated (2–8 keV) polarization degree (PD), $\sqrt{Q^2 + U^2}/I$, is 5.7%, below the MDP$_{99}$ (Weisskopf et al. 2010), which is about 20% for this observation and therefore not significant.[59] The PA $= \arctan(U/Q)/2$ is then unconstrained. The same conclusion is reached by applying an analysis as outlined by Strohmayer (2017) within XSPEC, which provides a PD ≈ 4.7%.

In order to test if a detectable polarization is present in some specific energy intervals, we performed an energy-resolved, phase-integrated (weighted) analysis in XSPEC. We started by dividing the IXPE working energy band into six equal bins (each 1 keV wide). The null hypothesis probability that the source is unpolarized in all energy bins is ≈22%.

We found a signal with PD $= 31.6\% \pm 10.5\%$ (slightly higher than the MDP$_{99}$) and PA $= -17.^{\circ}6^{+15.5}_{-15.0}$, computed east of north, in the 4–5 keV range. No significant polarization was detected in the remaining bins. In particular, we found only an upper limit of 23% and 45% (99% confidence level) in the two neighboring bins, 3–4 and 5–6 keV, respectively. Despite the fact that no firm conclusion can be reached about the trend of PD with energy, this may suggest that it increases in going from 3 to 4–5 keV. What happens at higher energies is harder to tell, essentially because the lower signal-to-noise ratio makes the MDP$_{99}$ higher, and this translates into a weaker constraint on PD.

In order to improve the counting statistics, we merged together the first two and the last three bins and considered the intervals 2–4, 4–5, and 5–8 keV. This did not produce any improvement, again resulting in an upper limit for PD of 24% and 55% (99% confidence level) at low and high energies, respectively. Figure 3 shows the contour plots of the PD and PA in each energy band obtained with the XSPEC `steppar` command by assuming the spectral model obtained from the XMM-Newton observation. A somewhat different choice for the boundaries of the central interval, e.g., taking the bin from 3.5 to 5 or 4 to 5.5 keV, yields consistent results.

[58] https://github.com/lucabaldini/ixpeobssim
[59] The minimum detectable polarization (MDP) is the largest signal expected to be produced by statistical fluctuations only at a given confidence level (usually 99%, MDP$_{99}$). The result of a polarization measurement is regarded as significant if it exceeds MDP$_{99}$.

We also attempted a phase-dependent analysis by folding the data at the spin period derived from the XMM-Newton timing and assuming $\dot{P} = 7.5 \times 10^{-11}$ s s^{-1} (see Section 3.1). No significant polarization was detected after dividing the pulse cycle into seven equally spaced phase bins. In the next step, we restricted to two phase bins, corresponding to the intervals [0.0, 0.38] and [0.38, 1.0], selected in such a way as to contain the secondary and primary peak of the pulse, respectively. Again, no polarization was measured, either considering the entire 2–8 keV band or restricting to low (2–4 keV) and high (4–8 keV) energies. A negative result was also found, limiting the analysis to the 4–5 keV range, where a phase-integrated signal was detected at a 99% confidence level. This was expected given that the detection is marginal even when all counts are considered.

An unbinned analysis (without background subtraction; González-Caniulef et al. 2023) in the 2–8 keV range shows that, when marginalized over the various parameters, the median PD is ≈8.4% and about 1σ above zero. This is somewhat less than the MDP_{99} of 10% for the observation without binning in phase or energy.

Fits to IXPE count spectra are rather inconclusive. Single-component models, either an (absorbed) BB or PL, provide a (formally) acceptable agreement with the data. However, the BB fit yields a column density of 2.7×10^{22} cm^{-2}, more than twice as low as that measured by XMM-Newton and previously reported in the literature. On the other hand, the parameters derived from the PL fit are consistent (within $\approx 1\sigma$) with those from the XMM-Newton BB+PL fit, but this just reflects the limited IXPE energy range (2–8 keV). When a single PL model is extended to the entire XMM-Newton energy band, the fit is no longer satisfactory (see Section 3.1). A fit with a two-component model (BB+BB or BB+PL) leaving all parameters free to vary is largely unconstrained, although freezing all of the parameters (except the normalizations) to those derived from the XMM-Newton data provides a good fit ($\chi^2 = 129.8$ for 162 dof).

A joint fit of the three Stokes parameters with the XSPEC model `phabs × (bbodyrad × polconst + powerlaw × polconst)`, again freezing all of the spectral parameters to those of the XMM-Newton analysis, does not provide any conclusive result. The upper limit (3σ confidence level) on the PD of the PL is about 57%, while the polarization of the BB is unconstrained. A similar conclusion is reached by truncating the PL at low energies. We remark that, while the fit is statistically acceptable in all of these cases, nothing can be said about the relative polarization direction between the two components.

4. Discussion

The IXPE observed SGR 1806–20 in two segments for a total exposure time of about 1 Ms in 2023 March–April. During the second stint, XMM-Newton targeted the source for about 45 ks to provide complementary spectral and timing information. Despite the renewed bursting activity, SGR 1806–20 was found at an (unabsorbed) flux level of 1.1×10^{-11} erg cm^{-2} s^{-1} in the 0.5–10 keV band, the lowest ever recorded, although still compatible within the uncertainties with the NuSTAR one reported by Younes et al. (2017). The XMM-Newton spectra are well fitted by an (absorbed) BB+PL model, and the spectral parameters ($kT_{\rm BB} = 0.6$ keV, $R_{\rm BB} = 1.3$ km, $\Gamma = 1.7$) are in broad agreement with those found by Younes et al. (2017). There is, however, a hint of a decrease of the BB radius with respect to the values measured by Younes et al. (2017) in 2015–2016, even if their NuSTAR data did not allow for a precise determination of the BB flux, and of a steepening of the PL with respect to the values measured by XMM-Newton in the same energy range prior to 2011 (Younes et al. 2015). The period and upper limit for $\dot{P}$ that we found are consistent with the past timing history of the source. The XMM-Newton pulse profile is double-peaked with a PF ≈ 5%, in agreement with previous measurements, while no pulsations were detected in the IXPE data.

The low flux level of SGR 1806–20 and the high background prevented a complete spectropolarimetric and timing analysis of IXPE data. No pulsations were detected, with an upper limit of 5.2% on the PF. Although poorly constrained, the IXPE spectrum is compatible with the BB+PL decomposition obtained from the analysis of XMM-Newton data. No significant polarization has been detected by integrating over the source rotational period and in the 2–8 keV energy band.

Interestingly, by restricting the analysis to the 4–5 keV range, we found a polarization signal that was significant at the 99% confidence level, with PD ≈ 32% and PA $\approx -18°$. At lower (2–4 keV) and higher (5–8 keV) energies, only upper limits can be derived on PD, with values at 3σ of 24% and 55%, respectively.

Although the XMM-Newton spectra are compatible with both a BB+PL and a BB+BB decomposition, the former is, in our opinion, favored, as discussed in Section 3.1. If the PL tail is associated with RCS, the predicted PD saturates at 33% in the energy interval where this component dominates (Taverna et al. 2020). The thermal emission can originate either from a magnetized, cooling atmosphere with PD ≈ 70%–80% (except for very peculiar viewing geometries; see, e.g., Taverna et al. 2015) or from the bare, condensed surface of the star, in which case a much lower PD $\lesssim$ 15%–20% is expected. It has also been proposed that radiation emerging from atmospheres heated from above by particle bombardment has a modest PD (comparable to that of the condensed surface; González-Caniulef et al. 2019; Doroshenko et al. 2022).

The constraints placed by the upper limits at low and high energies, together with a 99% confidence level PD of ≈32% at intermediate energies (where the thermal and nonthermal components coexist; see above), are compatible with a picture in which thermal emission comes from the bare neutron star surface or an atmosphere heated by backflowing particles. This scenario was also applied to 4U 0142+61, where a clear 90° swing of PA with energy was detected, signaling that radiation is dominated by O-mode photons (coming from the condensed surface/heated atmosphere) at low energies and X-mode photons (reprocessed by scatterings) at higher ones. The two sources may therefore be similar. Due to the low signal-to-noise ratio, no conclusion can be drawn about the dependence of the polarization direction on the energy and hence on which polarization mode is prevailing in a given energy range. However, emission from a condensed surface/heated atmosphere can be either mostly in the X- or in the O-mode (depending, e.g., on the orientation of the local magnetic field and the photon energy for the former and on the temperature gradient for the latter; see Taverna et al. 2022; Zane et al. 2023), so that a swing in PA is not necessarily expected.

Along this line, we explored a simple RCS model, in which thermal emission comes from two hot spots placed near the magnetic equator of the bare neutron star surface, including

vacuum birefringence. With this choice of the emission geometry (similar to that adopted for 4U 0142+61), radiation from the magnetic condensate exhibits a relatively large PD (≈20% in the O-mode) at low energies ($\lesssim$4 keV; Taverna et al. 2022). Since the magnetic field in the outer layers of a magnetar is expected to locally deviate from a dipole, the surface thermal map is likely different from the usual (dipolar) one, in which the hotter regions are around the magnetic poles, and may change in time (see Tiengo et al. 2013; Borghese et al. 2021, for some observational evidence; see also De Grandis et al. 2020, 2021 for theoretical considerations). Such a configuration indeed quantitatively reproduces both the observed XMM-Newton 1–10 keV spectrum and the 2–8 keV pulse profile, as well as being compatible with the IXPE detection/upper limits of PD in different energy bins (see Figure 3).

The low PF of SGR 1806–20 points to a sizable emitting surface area, as further supported by the inferred BB radius, ≈2 km, which is rather large compared to that usually seen in other magnetar sources ($R_{\rm BB} \approx 0.1$–1 km; Olausen & Kaspi 2014, and references therein). The actual size of the emitting region depends on the emission properties of the surface (and also on the geometry and viewing angle of the source). For poorly radiating surfaces, like a magnetic condensate, it is typically larger than $R_{\rm BB}$. In the model outlined above, the (total) size is ≈3.5 km for an assumed star radius of $R_{\rm NS} = 13$ km. The size of the emitting region is not, per se, a primary factor in establishing the intrinsic polarization properties of the source, which are mostly determined by the physical processes occurring in the surface/magnetosphere and by the source geometry. Indeed, replacing the magnetic condensate in our model with a fully ionized, magnetized H atmosphere produces a too-large PD at lower energies. On the other hand, the extent to which QED affects the observed polarization depends on the size of the emitting area. If radiation comes from a limited region, across which the direction of the B field changes little, vacuum birefringence produces almost no detectable effect; i.e., the predicted polarization at infinity is the same with or without QED. In case the emitting area has a size of $\approx R_{\rm NS}$, instead, the polarization computed without QED effects is quite a bit lower than that with QED. Despite SGR 1806–20 appearing promising in this respect, the low counting statistics prevented us from testing the QED versus no-QED scenario.

The quite large upper limit above ≈5 keV does not rule out different emission scenarios in which the PD is actually larger than ∼30%, the value predicted by saturated RCS. Phase-averaged values as high as ∼55%, for instance, may hint at the presence of hot gaseous caps on the star surface, as proposed by Zane et al. (2023) for 1RXS J1708. This possibility would still be consistent with the spectral properties of the source, given that a BB+BB model also provides a good representation of XMM-Newton spectra.

The IXPE observations of magnetars have clearly demonstrated the capabilities of polarization measurements in probing the physical conditions in strongly magnetized neutron stars. This includes the presence of QED effects, in favor of which indirect evidence was already gathered from the analysis of 4U 0142+61 and 1RXS J1708. The emerging picture shows substantial differences in the polarization pattern between 4U 0142+61 (and possibly SGR 1806–20) and 1RXS J1708, signaling that emission at higher energies (∼4–8 keV) may arise from different physical conditions in the different sources. As the case of SGR 1806–20 shows, collecting enough counts is crucial in providing clear-cut results. Further progress will require observing a larger sample of weaker sources, which will be possible for IXPE only with longer exposure times.

Acknowledgments

The Imaging X-ray Polarimetry Explorer (IXPE) is a joint US and Italian mission. The US contribution is supported by the National Aeronautics and Space Administration (NASA) and led and managed by its Marshall Space Flight Center (MSFC) with industry partner Ball Aerospace (contract NNM15AA18C). The Italian contribution is supported by the Italian Space Agency (Agenzia Spaziale Italiana, ASI) through contract ASI-OHBI-2017-12-I.0, agreements ASI-INAF-2017-12-H0 and ASI-INFN-2017.13-H0, and its Space Science Data Center (SSDC) with agreements ASI-INAF-2022-14-HH.0 and ASI-INFN 2021-43-HH.0, and by the Istituto Nazionale di Astrofisica (INAF) and the Istituto Nazionale di Fisica Nucleare (INFN). This research used data products provided by the IXPE Team (MSFC, SSDC, INAF, and INFN). R.Tu., R.Ta., and G.L.I. acknowledge financial support from the Italian MUR through grant PRIN 2017LJ39LM. G.L.I. also acknowledges financial support from INAF through grant "IAF-Astronomy Fellowships in Italy 2022—(GOG)." J.H. acknowledges support from the Natural Sciences and Engineering Council of Canada and the Canadian Space Agency. M.N. acknowledges support by NASA under award No. 80GSFC21M0002. T.T. was supported by grant JSPS KAKENHI JP19H05609. H.K. and E.G. acknowledge NASA support under grants 80NSSC18K0264, 80NSSC22K1291, 80NSSC21K1817, and NNX16AC42G. We thank N. Schartel for granting us XMM-Newton Director Discretionary Time.

Facilities: IXPE, XMM.

ORCID iDs

Roberto Turolla https://orcid.org/0000-0003-3977-8760
Roberto Taverna https://orcid.org/0000-0002-1768-618X
Gian Luca Israel https://orcid.org/0000-0001-5480-6438
Fabio Muleri https://orcid.org/0000-0003-3331-3794
Silvia Zane https://orcid.org/0000-0001-5326-880X
Matteo Bachetti https://orcid.org/0000-0002-4576-9337
Jeremy Heyl https://orcid.org/0000-0001-9739-367X
Alessandro Di Marco https://orcid.org/0000-0003-0331-3259
Ephraim Gau https://orcid.org/0000-0002-5250-2710
Henric Krawczynski https://orcid.org/0000-0002-1084-6507
Mason Ng https://orcid.org/0000-0002-0940-6563
Andrea Possenti https://orcid.org/0000-0001-5902-3731
Juri Poutanen https://orcid.org/0000-0002-0983-0049
Luca Baldini https://orcid.org/0000-0002-9785-7726
Giorgio Matt https://orcid.org/0000-0002-2152-0916
Michela Negro https://orcid.org/0000-0002-6548-5622
Iván Agudo https://orcid.org/0000-0002-3777-6182
Lucio A. Antonelli https://orcid.org/0000-0002-5037-9034
Wayne H. Baumgartner https://orcid.org/0000-0002-5106-0463
Ronaldo Bellazzini https://orcid.org/0000-0002-2469-7063
Stefano Bianchi https://orcid.org/0000-0002-4622-4240
Stephen D. Bongiorno https://orcid.org/0000-0002-0901-2097
Raffaella Bonino https://orcid.org/0000-0002-4264-1215
Alessandro Brez https://orcid.org/0000-0002-9460-1821

Niccolò Bucciantini https://orcid.org/0000-0002-8848-1392
Fiamma Capitanio https://orcid.org/0000-0002-6384-3027
Simone Castellano https://orcid.org/0000-0003-1111-4292
Elisabetta Cavazzuti https://orcid.org/0000-0001-7150-9638
Chieng-Ting Chen https://orcid.org/0000-0002-4945-5079
Stefano Ciprini https://orcid.org/0000-0002-0712-2479
Enrico Costa https://orcid.org/0000-0003-4925-8523
Alessandra De Rosa https://orcid.org/0000-0001-5668-6863
Ettore Del Monte https://orcid.org/0000-0002-3013-6334
Laura Di Gesu https://orcid.org/0000-0002-5614-5028
Niccolò Di Lalla https://orcid.org/0000-0002-7574-1298
Immacolata Donnarumma https://orcid.org/0000-0002-4700-4549
Victor Doroshenko https://orcid.org/0000-0001-8162-1105
Michal Dovčiak https://orcid.org/0000-0003-0079-1239
Steven R. Ehlert https://orcid.org/0000-0003-4420-2838
Teruaki Enoto https://orcid.org/0000-0003-1244-3100
Yuri Evangelista https://orcid.org/0000-0001-6096-6710
Sergio Fabiani https://orcid.org/0000-0003-1533-0283
Riccardo Ferrazzoli https://orcid.org/0000-0003-1074-8605
Javier A. Garcia https://orcid.org/0000-0003-3828-2448
Shuichi Gunji https://orcid.org/0000-0002-5881-2445
Wataru Iwakiri https://orcid.org/0000-0002-0207-9010
Svetlana G. Jorstad https://orcid.org/0000-0001-6158-1708
Philip Kaaret https://orcid.org/0000-0002-3638-0637
Vladimir Karas https://orcid.org/0000-0002-5760-0459
Fabian Kislat https://orcid.org/0000-0001-7477-0380
Jeffery J. Kolodziejczak https://orcid.org/0000-0002-0110-6136
Fabio La Monaca https://orcid.org/0000-0001-8916-4156
Luca Latronico https://orcid.org/0000-0002-0984-1856
Ioannis Liodakis https://orcid.org/0000-0001-9200-4006
Simone Maldera https://orcid.org/0000-0002-0698-4421
Alberto Manfreda https://orcid.org/0000-0002-0998-4953
Frédéric Marin https://orcid.org/0000-0003-4952-0835
Andrea Marinucci https://orcid.org/0000-0002-2055-4946
Alan P. Marscher https://orcid.org/0000-0001-7396-3332
Herman L. Marshall https://orcid.org/0000-0002-6492-1293
Francesco Massaro https://orcid.org/0000-0002-1704-9850
Tsunefumi Mizuno https://orcid.org/0000-0001-7263-0296
C.-Y. Ng https://orcid.org/0000-0002-5847-2612
Stephen L. O'Dell https://orcid.org/0000-0002-1868-8056
Nicola Omodei https://orcid.org/0000-0002-5448-7577
Chiara Oppedisano https://orcid.org/0000-0001-6194-4601
Alessandro Papitto https://orcid.org/0000-0001-6289-7413
George G. Pavlov https://orcid.org/0000-0002-7481-5259
Abel L. Peirson https://orcid.org/0000-0001-6292-1911
Matteo Perri https://orcid.org/0000-0003-3613-4409
Melissa Pesce-Rollins https://orcid.org/0000-0003-1790-8018
Pierre-Olivier Petrucci https://orcid.org/0000-0001-6061-3480
Maura Pilia https://orcid.org/0000-0001-7397-8091
Simonetta Puccetti https://orcid.org/0000-0002-2734-7835
Brian D. Ramsey https://orcid.org/0000-0003-1548-1524
John Rankin https://orcid.org/0000-0002-9774-0560
Ajay Ratheesh https://orcid.org/0000-0003-0411-4243
Oliver J. Roberts https://orcid.org/0000-0002-7150-9061
Roger W. Romani https://orcid.org/0000-0001-6711-3286
Carmelo Sgró https://orcid.org/0000-0001-5676-6214
Patrick Slane https://orcid.org/0000-0002-6986-6756
Paolo Soffitta https://orcid.org/0000-0002-7781-4104
Gloria Spandre https://orcid.org/0000-0003-0802-3453
Douglas A. Swartz https://orcid.org/0000-0002-2954-4461
Toru Tamagawa https://orcid.org/0000-0002-8801-6263
Fabrizio Tavecchio https://orcid.org/0000-0003-0256-0995
Allyn F. Tennant https://orcid.org/0000-0002-9443-6774
Nicholas E. Thomas https://orcid.org/0000-0003-0411-4606
Francesco Tombesi https://orcid.org/0000-0002-6562-8654
Alessio Trois https://orcid.org/0000-0002-3180-6002
Sergey S. Tsygankov https://orcid.org/0000-0002-9679-0793
Jacco Vink https://orcid.org/0000-0002-4708-4219
Martin C. Weisskopf https://orcid.org/0000-0002-5270-4240
Kinwah Wu https://orcid.org/0000-0002-7568-8765
Fei Xie https://orcid.org/0000-0002-0105-5826

References

Arnaud, K. A. 1996, in ASP Conf. Ser. 101, Astronomical Data Analysis Software and Systems V, ed. G. H. Jacoby & J. Barnes (San Francisco, CA: ASP), 17
Atteia, J. L., Boer, M., Hurley, K., et al. 1987, ApJL, 320, L105
Bachetti, M., Maccarone, T. J., Brightman, M., et al. 2020, ApJ, 891, 44
Bachetti, M., Pilia, M., Huppenkothen, D., et al. 2021, ApJ, 909, 33
Baldini, L., Bucciantini, N., Di Lalla, N., et al. 2022, SoftX, 19, 101194
Bibby, J. L., Crowther, P. A., Furness, J. P., & Clark, J. S. 2008, MNRAS, 386, L23
Borghese, A., Rea, N., Turolla, R., et al. 2021, MNRAS, 504, 5244
Brivio, R., Ferro, M., Palmer, D. M., et al. 2023, GCN, 33451, 1
Buccheri, R., Bennett, K., Bignami, G. F., et al. 1983, A&A, 128, 245
Caiazzo, I., González-Caniulef, D., Heyl, J., & Fernández, R. 2022, MNRAS, 514, 5024
De Grandis, D., Taverna, R., Turolla, R., et al. 2021, ApJ, 914, 118
De Grandis, D., Turolla, R., Wood, T. S., et al. 2020, ApJ, 903, 40
Di Marco, A., Costa, E., Muleri, F., et al. 2022, AJ, 163, 170
Di Marco, A., Soffitta, P., Costa, E., et al. 2023, AJ, 165, 143
Doroshenko, V., Poutanen, J., Tsygankov, S. S., et al. 2022, NatAs, 6, 1433
Duncan, R. C., & Thompson, C. 1992, ApJL, 392, L9
Fernández, R., & Davis, S. W. 2011, ApJ, 730, 131
Fernández, R., & Thompson, C. 2007, ApJ, 660, 615
González-Caniulef, D., Caiazzo, I., & Heyl, J. 2023, MNRAS, 519, 5902
González-Caniulef, D., Zane, S., Turolla, R., & Wu, K. 2019, MNRAS, 483, 599
Heyl, J. S., & Shaviv, N. J. 2000, MNRAS, 311, 555
Heyl, J. S., & Shaviv, N. J. 2002, PhRvD, 66, 023002
Hurley, K., Boggs, S. E., Smith, D. M., et al. 2005, Natur, 434, 1098
Kaspi, V. M., & Beloborodov, A. M. 2017, ARA&A, 55, 261
Kouveliotou, C., Norris, J. P., Cline, T. L., et al. 1987, ApJL, 322, L21
Lai, D. 2023, PNAS, 120, e2216534120
Laros, J. G., Fenimore, E. E., Klebesadel, R. W., et al. 1987, ApJL, 320, L111
Mazets, E. P., Golenetskii, S. V., Ilinskii, V. N., et al. 1981, Ap&SS, 80, 3
Mereghetti, S., Gotz, D., Ferrigno, C., et al. 2023, GCN, 33494, 1
Mereghetti, S., Götz, D., Mirabel, I. F., & Hurley, K. 2005a, A&A, 433, L9
Mereghetti, S., Tiengo, A., Esposito, P., et al. 2005b, ApJ, 628, 938
Nobili, L., Turolla, R., & Zane, S. 2008, MNRAS, 386, 1527
Olausen, S. A., & Kaspi, V. M. 2014, ApJS, 212, 6
Palmer, D. M., Barthelmy, S., Gehrels, N., et al. 2005, Natur, 434, 1107
Santangelo, A., Zane, S., Feng, H., et al. 2019, SCPMA, 62, 29505
Strohmayer, T. E. 2017, ApJ, 838, 72
Strüder, L., Briel, U., Dennerl, K., et al. 2001, A&A, 365, L18
Taverna, R., Muleri, F., Turolla, R., et al. 2014, MNRAS, 438, 1686
Taverna, R., Turolla, R., Gonzalez Caniulef, D., et al. 2015, MNRAS, 454, 3254
Taverna, R., Turolla, R., Muleri, F., et al. 2022, Sci, 378, 646
Taverna, R., Turolla, R., Suleimanov, V., Potekhin, A. Y., & Zane, S. 2020, MNRAS, 492, 5057
Thompson, C., & Duncan, R. C. 1993, ApJ, 408, 194

Thompson, C., Lyutikov, M., & Kulkarni, S. R. 2002, ApJ, 574, 332
Tiengo, A., Esposito, P., Mereghetti, S., et al. 2013, Natur, 500, 312
Turner, M. J. L., Abbey, A., Arnaud, M., et al. 2001, A&A, 365, L27
Turolla, R., Zane, S., & Watts, A. L. 2015, RPPh, 78, 116901
van Adelsberg, M., & Perna, R. 2009, MNRAS, 399, 1523
Vaughan, B. A., van der Klis, M., Wood, K. S., et al. 1994, ApJ, 435, 362
Weisskopf, M. C., Guainazzi, M., Jahoda, K., et al. 2010, ApJ, 713, 912
Weisskopf, M. C., Soffitta, P., Baldini, L., et al. 2022, JATIS, 8, 026002
Woods, P. M., Kouveliotou, C., Finger, M. H., et al. 2007, ApJ, 654, 470
Younes, G., Baring, M. G., Kouveliotou, C., et al. 2017, ApJ, 851, 17
Younes, G., Kouveliotou, C., & Kaspi, V. M. 2015, ApJ, 809, 165
Zane, S., Taverna, R., González-Caniulef, D., et al. 2023, ApJL, 944, L27